Journal of Solid State Chemistry **165,** 247–253 (2002)
doi:10.1006/jssc.2002.9512, available online at http://www/idealibrary.com on IDEAL®

# Sol–Gel Template Synthesis of Highly Ordered $LiCo_{0.5}Mn_{0.5}O_2$ Nanowire Arrays and Their Structural Properties

Yingke Zhou and Hulin Li[1]

*Chemistry Department of Lanzhou University, Lanzhou 730000, People's Republic of China*

Received August 29, 2001; in revised form December 28, 2001; accepted January 18, 2002; published online March 27, 2002

**Highly ordered $LiCo_{0.5}Mn_{0.5}O_2$ nanowire arrays were prepared using porous anodic aluminum oxide (AAO) template from sol–gel solution containing $Li(CH_3COO)$, $Co(CH_3COO)_2$, and $Mn(CH_3COO)_2$. Electron microscope results showed that uniform length and diameter of $LiCo_{0.5}Mn_{0.5}O_2$ nanowires were obtained, and the length and diameter of $LiCo_{0.5}Mn_{0.5}O_2$ nanowires are dependent on the pore diameter and the thickness of the applied AAO template. X-ray diffraction and electron diffraction pattern investigations demonstrate that $LiCo_{0.5}Mn_{0.5}O_2$ nanowires are a layered structure of $LiCo_{0.5}Mn_{0.5}O_2$ crystal. X-ray photoelectron spectroscopy analysis indicates that the most closely resembling stoichiometric layered $LiCo_{0.5}Mn_{0.5}O_2$ material has been obtained.** © 2002 Elsevier Science (USA)

*Key Words:* **$LiCo_{0.5}Mn_{0.5}O_2$; nanowire arrays; lithium-ion batteries; AAO template; sol–gel.**

## 1. INTRODUCTION

Many lithium-intercalated transition metal oxides have been studied as positive electrode materials in high-energy-density rechargeable batteries. Research work in this area has focused mainly on $LiMn_2O_4$ and $LiMO_2$ ($M$ = Ni,Co) compounds synthesized by solid reaction using high-temperature (HT) methods (1–9), which show higher operating voltages than the conventional 3-V systems. These compounds crystallize in the spinel type (10) and the $\alpha$-$NaFeO_2$ layered structure (11), respectively. Lithium cobaltate is one of the most advanced materials studied but some limitations are due to its high cost, moderate capacity, and toxicity. Lithium nickelate is one of the most attractive materials for lithium-ion cells. However, non-stoichiometric $Li_xNi_y^{(II)}Ni_{1-y}^{(III)}O_2$ oxides are usually obtained; nickel dioxide electrochemically formed from $LiNiO_2$ is quite active for an organic electrolyte oxidation and the reaction is exothermic. Lithiated manganese oxide, $LiMn_2O_4$, is exploited very much as a battery cathode in lithium-ion cells due to its avaibility and nontoxicity, besides its low cost compared to counterpart materials such as $LiCoO_2$ and $LiNiO_2$. However, the $LiMn_2O_4$ spinel phase exhibits lower capacity and the rechargeable capacity fades rapidly for deep charge–discharge cycles, particularly at high temperature (60°C). $LiMnO_2$ is also a candidate positive electrode for lower cost and higher capacity lithium-ion batteries; many attempts have been made to prepare layered $LiMnO_2$, mainly involving the use of aqueous media (12–14). The resulting products, though interesting, have stoichiometries which differ from that of $LiMnO_2$, contain water or protons, are of poor crystallinity, or do not maintain their structure during cycling.

A possible solution to reducing the above disadvantages is to utilize a solid solution of the general formula $LiCo_{1-y}Mn_yO_2$, which are isostructural with the layered oxide end-compounds and showed electrochemical features better than those of $LiCoO_2$ and $LiMnO_2$ (15–17). In recent years, nanostructured electrode materials have attracted great interest since the capacity of electrode material is critically affected by the morphology of the materials which contribute to different ways of diffusion processes of $Li^+$ ion (18). The nanostructured materials have been explored for use as cathode and anode materials in lithium-ion battery in recent years. Novel nanostructured electrode material is not only a good model system for the research of intercalation reaction of $Li^+$, but also a promising material in some special Li-ion battery systems such as microbatteries. As an important preparation method of nanostructured materials, template methods (19) have successfully played crucial role in a variety of areas. Different kinds of template such as anodic porous alumina, polymer, and nanochannel glass templates have been widely investigated. Normally anodized aluminum in appropriate acid solution forms anodic porous alumina template. Compared with other templates, the size of holes of the template can be readily controlled by properly

[1]To whom correspondence should be addressed. Fax: +86-931-891-2582. Email: lihl@lzu.edu.cn.



0022-4596/02 $35.00

adjusting the condition of anodization (20). In this paper, we firstly apply sol–gel template method to prepare $LiCo_{0.5}Mn_{0.5}O_2$ as highly ordered nanowire arrays, which are distinctly different from the results of conventional methods.

Sol–gel chemistry has recently evolved as a powerful approach for preparing inorganic materials such as glasses and ceramics (21–23). This method for the synthesis of inorganic materials has a number of advantages over more conventional synthetic procedures. For example, high-purity materials can be synthesized at a lower temperature. In addition, homogeneous multicomponent systems can be obtained by mixing precursor solutions. This allows for easy chemical doping of the materials prepared. Finally, the rheological properties of the sol and the gel can be utilized in processing the material, by dip coating of thin films, spinning of fibers, etc. (23, 24). Here we have combined the concepts of sol–gel synthesis and template preparation of nanomaterials to yield a new general route for preparing $LiCo_{0.5}Mn_{0.5}O_2$ nanoarrays. This was accomplished by conducting sol–gel synthesis within the pores of various nanoporous membranes, and monodispersed nanoarrays of $LiCo_{0.5}Mn_{0.5}O_2$ nanowires are obtained.

## 2. EXPERIMENTAL

### 2.1. Membrane Preparation

High-purity aluminum sheets (99.99%, 20 mm × 10 mm) were employed in this experiment. Prior to anodization, the metal surfaces were degreased, etched in alkaline solution, rinsed in distilled water, and electropolished to achieve a smooth surface. It was necessary to immerse the samples in concentrated acid or alkaline solution for several minutes to remove the oxide layer formed during the electropolishing process. All samples were rinsed in distilled water and then transferred to a nitrogen environment. The resultant clean aluminum samples were anodized at constant potential in phosphoric acid (99–101V, 0°C, Pt sheet as a counter electrode). Then the whole sheet was placed into saturated $HgCl_2$ solution to separate the template membrane from the Al substrate. The membrane was rinsed with distilled water and then immersed in 5% $H_3PO_4$ solution at 30°C for about 30 min in order to dissolve the barrier-type part on the bottom of the nanoholes. AAO templates were characterized by using transmission electron microscopy (TEM) and scanning electron microscopy (SEM).

### 2.2. Preparation of $LiCo_{0.5}Mn_{0.5}O_2$ Nanowire Arrays

Metal acetates were used as the cationic sources, and citric acid and ethylene glycol as the monomers for forming the polymeric matrix. A 1:1:2 molar ratio of $Co(CH_3COO)_2$, $Mn(CH_3COO)_2$, and $Li(CH_3COO)$ was dissolved in a mixture of citric acid and ethylene glycol (1 : 4 molar ratio). A clear solution was then produced, and it was heated at 140°C to induce esterification and distill out excess ethylene glycol. Thus the sol was obtained.

The alumina template membrane was dipped into the sol for the desired amount of time and removed, and the excess sol on the membrane surface was wiped off using a laboratory tissue, followed by drying under vacuum at 50°C for 1 h. The membrane surface was carefully wiped again to remove salts crystallized on the surface and heated at 600°C for 10 h in open air, resulting in formation of arrays of $LiCo_{0.5}Mn_{0.5}O_2$ nanowires in the inside of the pores of the AAO template.

### 2.3 Characterization of $LiCo_{0.5}Mn_{0.5}O_2$ Nanowire Arrays

The structure and morphology properties of $LiCo_{0.5}Mn_{0.5}O_2$ nanowire arrays were characterized by several techniques. X-ray diffraction (XRD) data of the template membrane were collected using a Rigaku D/MAX2400 diffractometer with Cu-$K\alpha$ radiation ($\lambda = 1.54056$ Å) and a graphite monochromator at 40 kV, 80 mA. The step scanning mode was used with a step of 0.02° and the data were acquired in the $2\theta$ range 10°–80°. The TEM (Hitachi 600, Japan) was used to observe the morphology and degree of agglomeration. The accelerating voltage of the electron beam was 100 kV, and the camera length was 80 cm. A gold single crystal was used as a standard to check the camera length. Before TEM observation the alumina template membrane was dissolved by using 3M NaOH, and then diluted with distilled water three times. Scanning electron microscopic (SEM) images were recorded with JSM-5600LV microscope at an acceleration voltage of 20 kV. For SEM sample, the alumina template membrane was attached to a Cu cylinder. Then two drops of 3 M NaOH were dropped on the sample to dissolve the partial membrane, and the samples were sputter-coated with gold before the SEM measurement in order to increase their conductivity. The X-ray photoelectron spectroscopy (XPS) data were obtained by a V. G. ESCA Lab. 2201-XL photoelectron spectrometer with a Mg$K\alpha$ source, a concentric hemispherical analyzer operating in fixed analyzer transmission mode, and a multichannel detector. The pressure in the analysis chamber was less than $2 \times 10^{-10}$ Torr. The spectra were acquired with 50 eV pass energy and 1 $mm^2$ spot (large area mode without using XL lens). The binding energy was calibrated with reference to the C1$s$ level of carbon (285.0 eV).

## 3. RESULTS AND DISCUSSION

### 3.1. TEM and SEM Analysis

When anodized in an acidic electrolyte, aluminum forms a porous oxide with very uniform and parallel pores open

at one end but sealed at the other (25–27). Its structure is described as a close-packed array of columnar cells, each containing a central pore the side and interval of which can be controlled by changing the forming conditions (25–27). Figure 1a presents the TEM photograph of a porous AAO template with a pore diameter $d$ of $100 \pm 5$ nm and a pore density of about $10^9$–$10^{10}$ cm$^{-2}$. Perfect hexagonal pore arrays can be observed within domains of microsize, which are separated from neighboring aluminum oxide domains with a different orientation of the pore lattice by grain boundaries. Thus, a polycrystalline pore structure is observed. As a further observation, the SEM photograph in Fig. 1b depicts the cross section of the AAO template with pores parallel to each other and perpendicular to the surface of the membrane.

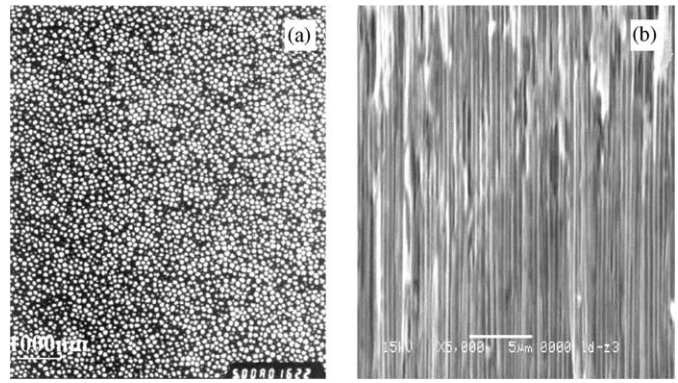


**FIG. 1.** TEM photograph of AAO template (a) and SEM photograph of AAO template (b).

The TEM images of $LiCo_{0.5}Mn_{0.5}O_2$ nanowires formed by the AAO template are shown in Fig. 2. The as-produced nanowires are uniformly distributed and have a diameter of around 100 nm. The length and the diameter of these nanowires correspond exactly to that of the templates. Figures 2a and 2b showed TEM images of three major $LiCo_{0.5}Mn_{0.5}O_2$ nanowires at light and dark field, respectively. We can see that these images are of the same three $LiCo_{0.5}Mn_{0.5}O_2$ nanowires, and three other nanowires in this image are only partially observed. There are many bright little dots in the nanowire of Fig. 2b, which indicates

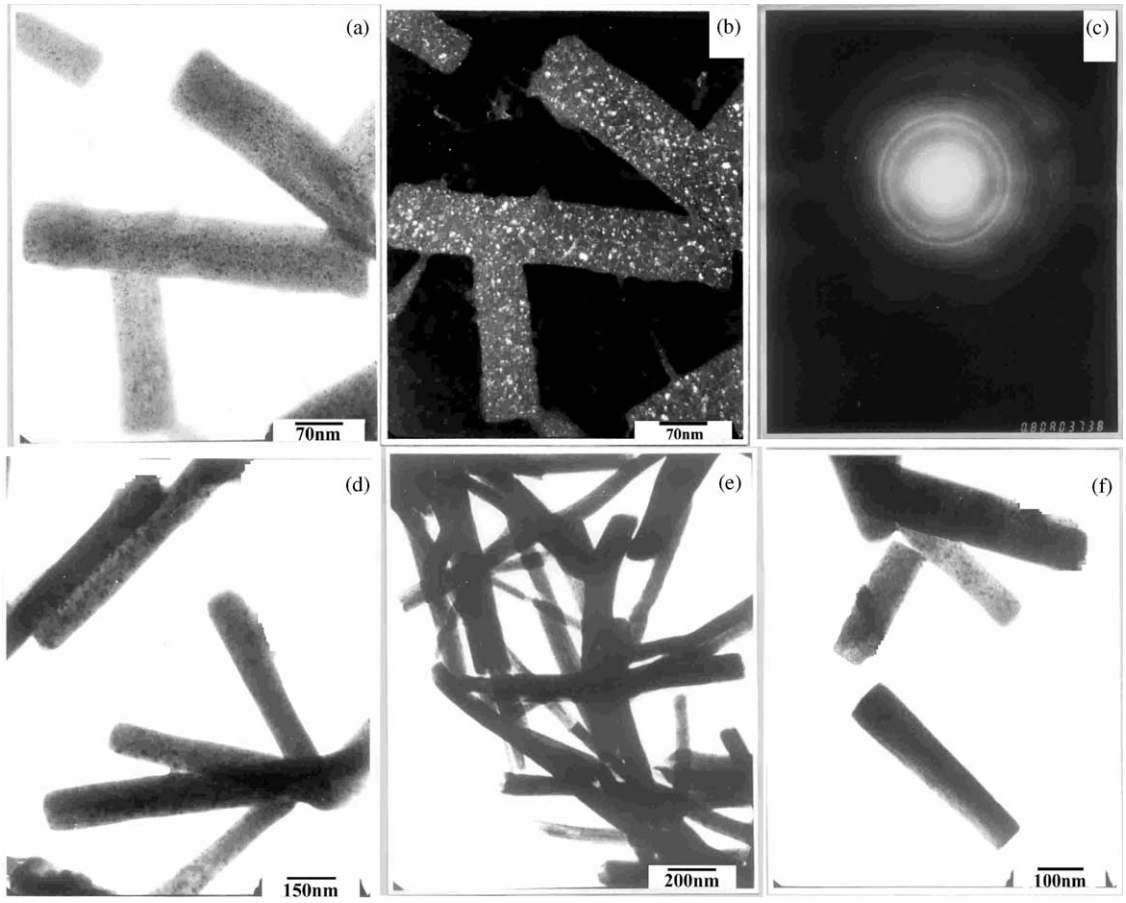


**FIG. 2.** TEM photographs of $LiCo_{0.5}Mn_{0.5}O_2$ nanometer wires: (a–c) The bright field TEM image, dark field TEM image, and corresponding electron diffraction pattern; (d) TEM image of several $LiCo_{0.5}Mn_{0.5}O_2$ nanowires; (e, f) more TEM images of $LiCo_{0.5}Mn_{0.5}O_2$ nanowires.

that $LiCo_{0.5}Mn_{0.5}O_2$ nanowire consists of many little crystals, and these bright crystals exactly diffracted out from this angle when this image is taken. Here we can conclude that the $LiCo_{0.5}Mn_{0.5}O_2$ nanowire obtained in our experiment is polycrystalline. The corresponding electron diffraction pattern taken from these $LiCo_{0.5}Mn_{0.5}O_2$ nanowires is shown in Fig. 2c. The diffraction spots correspond to the (003), (101), (104), and (110) diffraction planes of layered $LiCo_{0.5}Mn_{0.5}O_2$ crystalline according to the electron diffraction formula. Figure 2d shows six $LiCo_{0.5}Mn_{0.5}O_2$ nanowires, in which two nanowires contact and keep parallel to each other; the reason is that the alumina matrix between them is not dissolved completely, and makes them keep the same parallel situation as in the template. The other four also adhere together at the bottom and form a cluster of nanowires. The reason is the same as above. This image also shows these nanowires have uniform length and diameter, which corresponding pores of the employed AAO template. A large number of nanowires are shown in Fig. 2e. These nanowires cross, contact, and overlap with each other, and we cannot distinguish one from the others. Figure 2f shows another image of four $LiCo_{0.5}Mn_{0.5}O_2$ nanowires.

Figure 3 presents SEM images of $LiCo_{0.5}Mn_{0.5}O_2$ nanowires grown by AAO template. These photographs show the nanowires are parallel to each other, and few microscopic defects are found in them. Figure 3a presents several clusters of $LiCo_{0.5}Mn_{0.5}O_2$ nanowires, the alumina matrix of which is almost dissolved completely, and only the bottom adhere together due to the residual alumina, to make several nanowires form a cluster. From each cluster of these nanowires, we can see that both the top surface and the cross section of the $LiCo_{0.5}Mn_{0.5}O_2$ nanowire arrays were obtained and these nanowires are parallel to each other, uniformly distributed, and highly ordered and few microscopic defects are found in these wires. This is because the residual alumina matrix makes the nanowires still keep the situations within the pores of the nanoporous alumina matrix. In addition, we can conclude that the rigidity of the nanowires is strong, and they keep standing straight from the bottom even when it is alone and no alumina to rely on. Figure 3b is taken at a lower multiple and the visual field is larger than that of Fig. 3a, and

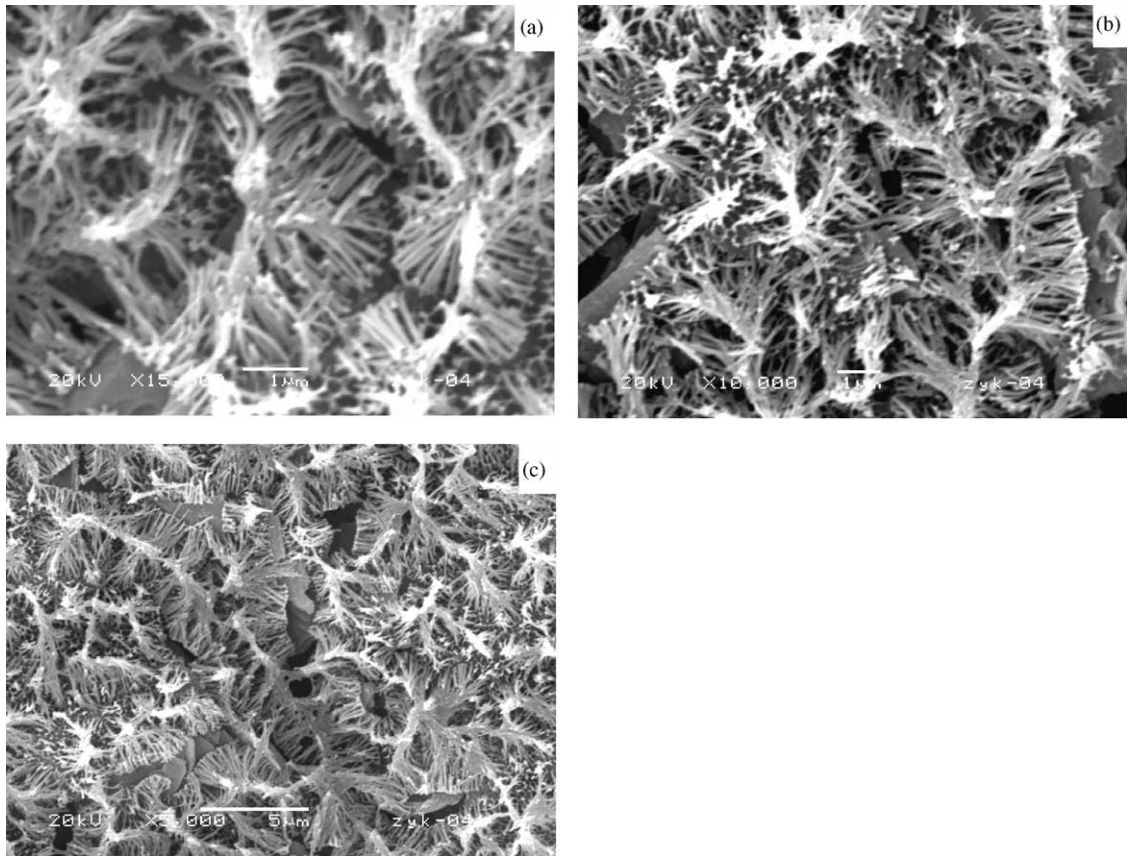


**FIG. 3.** SEM photographs of $LiCo_{0.5}Mn_{0.5}O_2$ nanowire arrays: (a) clusters of $LiCo_{0.5}Mn_{0.5}O_2$ nanowires; (b) magnified local image from (a) of $LiCo_{0.5}Mn_{0.5}O_2$ nanowire arrays; (c) further magnified local image from (b) of $LiCo_{0.5}Mn_{0.5}O_2$ nanowire arrays.

Fig. 3c has still more enlarged visual fields than Fig. 3b. From these we find that a $LiCo_{0.5}Mn_{0.5}O_2$ nanowire array can be produced in large areas within the pores of the AAO template. As a result, the lengths of $LiCo_{0.5}Mn_{0.5}O_2$ nanowires are equivalent to the thickness of the applied template, and at the same time the outside diameters of these wires are equivalent to the pore diameter of the template membrane (100 nm).

### 3.2. XRD Analysis

The ideal layered $LiCo_{0.5}Mn_{0.5}O_2$ has a rock salt structure with lithium and transition metal cations occupying alternative layers of octahedral sites (3a and 3b sites, respectively) in a distorted cubic close-packed oxygen ion lattice (6c site) (28–30). In space-group notation, this corresponds to the trigonal space group *R*-3*m*. The structure of layered $LiCo_{0.5}Mn_{0.5}O_2$ should be similar to layered $LiCoO_2$ with a rhombohedral unit cell (*R*-3*m*), although a rock-type structure (F*m*3*m*) appeared in the $LiCo_{0.5}Mn_{0.5}O_2$ via a solid state reaction (31). The XRD spectrum of $LiCo_{0.5}Mn_{0.5}O_2$ nanowires (within the AAO template) is shown in Fig. 4 and the major diffraction peak positions of $LiCoO_2$ (JCPDS, card no: 16-0427), $LiMnO_2$ (JCPDS, card no: 35-0749) and the observed peak positions of $LiCo_{0.5}Mn_{0.5}O_2$ from Fig. 4 are listed in Table 1. From these information, the X-ray patterns of $LiCo_{0.5}Mn_{0.5}O_2$ can be indexed to a rhombohedral unit cell (*R*-3*m*), and they are similar to the layered $LiCo_yMn_{1-y}O_2$ reported previously (31). Although because the background diffraction peaks of $Al_2O_3$ template are very large, only the major diffraction peaks of $LiCo_{0.5}Mn_{0.5}O_2$ are observed and the others may be annihilated by the background diffraction of $Al_2O_3$, the occurred peaks are closely corresponding to layered $LiCo_{0.5}Mn_{0.5}O_2$ (003), (101), and (104) planes. We can also see that all the diffraction peaks intensity of $LiCo_{0.5}Mn_{0.5}O_2$ is smaller

**TABLE 1**
**Major Diffraction Peak Positions of Layered $LiCoO_2$ (*R*-3*m*) and $LiMnO_2$ (*Pmnm*) and Observed Peak Positions of $LiCo_{0.5}Mn_{0.5}$ from Fig. 4**

| $LiCoO_2$ | | $LiMnO_2$ | | $LiCo_{0.5}Mn_{0.5}O_2$ | |
|---|---|---|---|---|---|
| 2$\theta$ | (*hkl*) | 2$\theta$ | (*hkl*) | 2$\theta$ | (*hkl*) |
| 18.947 | 003 | 15.417 | 010 | 19.034 | 003 |
| 37.425 | 101 | 24.863 | 110 | 36.913 | 101 |
| 39.132 | 012 | 35.600 | 011 | 39.887 | 012 |
| 45.281 | 104 | 36.924 | 120 | 44.798 | 104 |
| 49.468 | 015 | 37.597 | 101 | 49.535 | 015 |
| 59.640 | 107 | 39.382 | 200 | | |
| 65.494 | 018 | 40.853 | 111 | | |
| 66.110 | 110 | 42.536 | 210 | 66.547 | 110 |
| 69.699 | 113 | 45.140 | 021 | | |

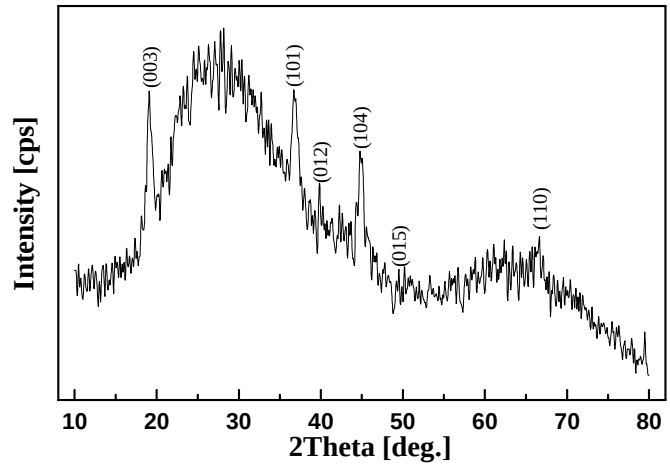


**FIG. 4.** XRD patterns of $LiCo_{0.5}Mn_{0.5}O_2$/alumina composite membrane.

than that of amorpha $Al_2O_3$. The reason for weaker diffraction peaks of $LiCo_{0.5}Mn_{0.5}O_2$ derives from a little quantity of $LiCo_{0.5}Mn_{0.5}O_2$ in template and $LiCo_{0.5}Mn_{0.5}O_2$ were not covered on the surface of template.

### 3.3. XPS Analysis

The chemical composition of layered $LiCo_{0.5}Mn_{0.5}O_2$ nanowire arrays (within the AAO template) was obtained by XPS measurements. In an X-ray photoelectron spectroscopy (XPS) experiment, the samples are exposed to monochromic X-radiation and the properties of the inner-shell electrons are probed. The quantitative analysis of the $LiCo_{0.5}Mn_{0.5}O_2$ is made from the integrated intensities of the Co2*p*, Mn2*p*, and Li1*s* lines, which are observed with the peaks attributed to oxygen in the XPS spectrum. Of course, the peaks corresponding to aluminium are also recorded in the spectrum. Figures 5a–5e display the XPS spectra of Mn2*p*, Co2*p*, Li1*s*, O1*s*, and Al2*p* core levels, respectively, for $LiCo_{0.5}Mn_{0.5}O_2$/AAO composite. The line of Li1*s* core level has a low intensity with a binding energy located at 54.1 eV (Fig. 5c). The line shape of the core levels O1*s* and Al2*p* are Gaussian-like with binding energy of 530.1 eV (Fig. 5d) and 74.0 eV (Fig. 5e), respectively. We can see the peak intensities of O1*s* and Al2*p* are larger than those of the other elements, and this is in accord with the XRD analysis. The peaks located at 780.1 eV and 795.6 eV (Fig. 5b) are attributed to the spin–orbit splitting of the Co2*p* components, $Co2p_{3/2}$ and $Co2p_{1/2}$, respectively. The entire 2*p* region has to be included for quantitative analysis, because the total amount of the respective ion species is equal to the integral number over all Co2*p* states. Peaks of the Co2*p* are close to those previously reported (32), and we think that the Co ion is in a trivalent $Co^{3+}$ low-spin state. An energy

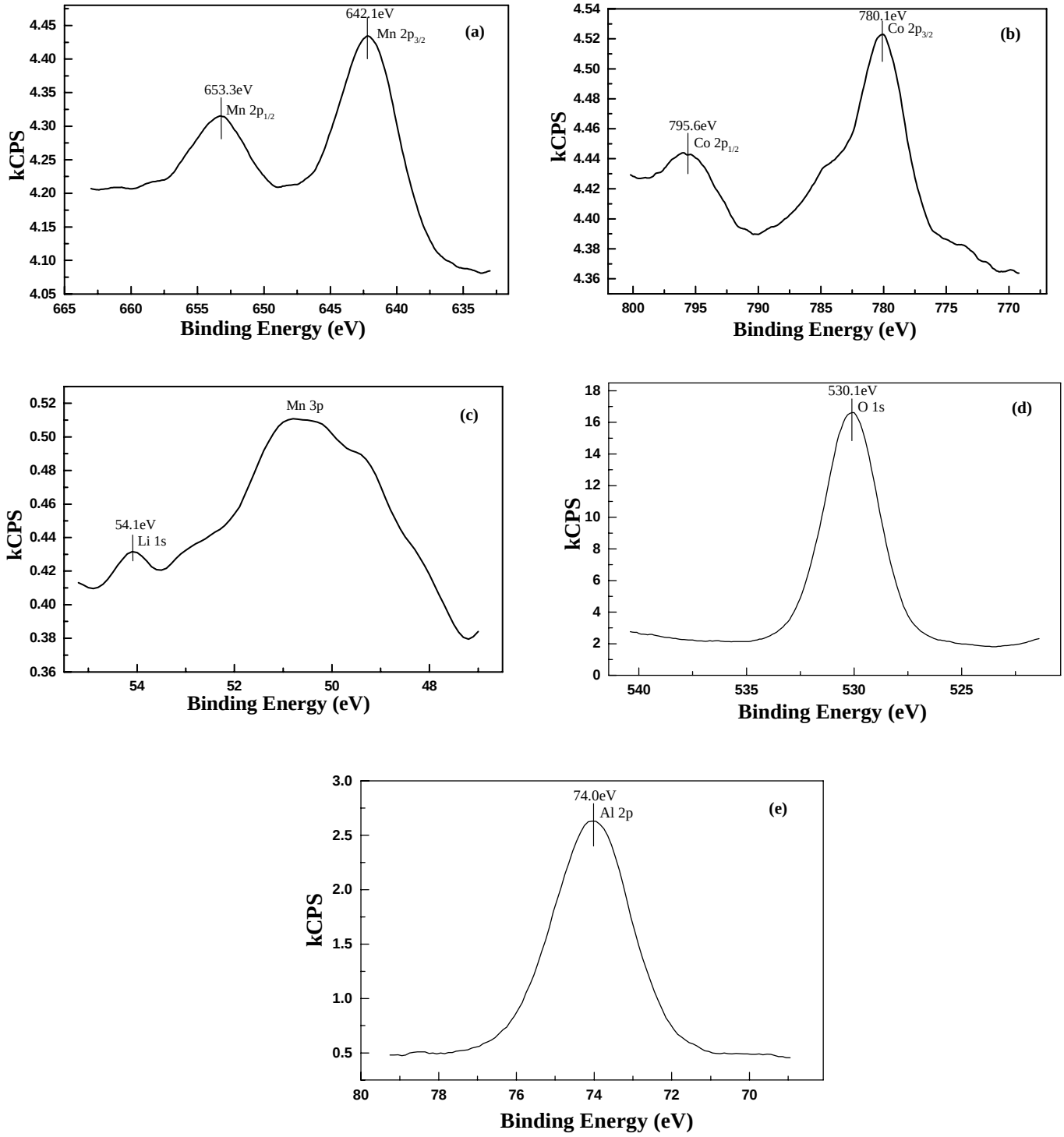


**FIG. 5.** XPS spectra of (a) Mn2*p*; (b) Co2*p*; (c) Li1*s*; (d) O1*s* and (e) Al2*p* core levels for $LiCo_{0.5}Mn_{0.5}O_2$/alumina composite membrane.

separation of 11.2 eV is observed between the Mn2$p_{3/2}$ and Mn2$p_{1/2}$ states (Fig. 5a). Thus, the Mn2$p_{3/2}$ peak in $LiCo_{0.5}Mn_{0.5}O_2$ is observed between those of $MnO_2$ (642.6 eV) and $Mn_2O_3$ (641.6 eV). For the peak integration, the area under each peak was integrated to obtain the peak intensity. As the element O corresponds to both $Al_2O_3$ and $LiCo_{0.5}Mn_{0.5}O_2$, we integrated the whole O peak intensity, from which the part corresponding to $Al_2O_3$ was

subtracted (the Al amount was determined from the integrated peak intensity of the Al peak in Fig. 5e), and the residual part was applied in the quantitative analysis of O in $LiCo_{0.5}Mn_{0.5}O_2$. The integration results show peak intensities: Mn (1.492); Co (2.148); Li (0.0341); O (39.756); Al (6.798). Then with these peak intensities, we apply the element-sensitive factor method (33) to obtain the ratio of these elements' amounts. The intensity ratio between XPS peaks Mn2*p*, Co2*p*, Li1*s*, and O1*s* (after subtraction) shows that the $LiCo_{0.5}Mn_{0.5}O_2$ product has been synthesized and most closely resembles stoichiometric layered material.

## 4. CONCLUSION

$LiCo_{0.5}Mn_{0.5}O_2$ nanowire arrays were successfully fabricated by a sol–gel template process. Investigations of X-ray diffraction and electron diffraction patterns demonstrated that $LiCo_{0.5}Mn_{0.5}O_2$ nanowires are a layered structure of $LiCo_{0.5}Mn_{0.5}O_2$ crystal. Electron microscope results show that these $LiCo_{0.5}Mn_{0.5}O_2$ nanowires have a uniform length and diameter and form a highly ordered array, and this is determined by the pore diameter and the thickness of the applied AAO template. XPS analysis indicates that the nanowires most closely resemble stoichiometric layered material.

## ACKNOWLEDGMENTS

This work is supported by Nation Natural Science Foundation of China (No. 69871013). We would like to express our sincere thanks to Chief Engineer Gui-Xun Cao of Gansu Instrumental Analysis&Research Center for TEM measurement and analysis, to Chief Engineer Da-Kang Song of Material Department of Lanzhou University for measurement and analysis of XRD data.

## REFERENCES

1. J. C. Hunter, *J. Solid State Chem.* **39,** 142 (1981).
2. M. M. Thackeray, W. I. F. David, P. G. Bruce, and J. B. Goodenough, *Mater. Res. Bull.* **18,** 461 (1983).
3. J. M. Tarascon and D. Guyomard, *J. Electrochem. Soc.* **138,** 2864 (1991).
4. T. Ohzuku, M. Kitagawa, and T. Hirai, *J. Electrochem. Soc.* **137,** 769 (1990).
5. J. M. Tarascon, D. Guyomard, and G. L. Baker, *J. Power Sources.* **43–44,** 689 (1993).
6. K. Mizushina, P. C. Jones, P. J. Wiseman, and J. B. Goodenough, *Mater. Res. Bull.* **15,** 783 (1980).
7. E. Rosen, J. N. Reimers, and J. R. Dahn, *Solid State Ionics* **62,** 53 (1993).
8. P. Barboux, J. M. Tarascon, and F. K. Shokoohi, *J. Solid State Chem.* **94,** 185 (1991).
9. I. Saadoune and C. Delmas, *J. Mater. Chem.* **6,** 193 (1996).
10. Y. Gao and J. R. Dahn, *J. Electrochem. Soc.* **143,** 100 (1996).
11. A. Ueda and T. Ohzuku, *J. Electrochem. Soc.* **141,** 2013 (1994).
12. M. H. Rossouw and M. M. Thackeray, *J. Solid State Chem.* **104,** 464 (1995).
13. M. M. Thackeray, *J. Electrochem. Soc.* **142,** 2558 (1995).
14. F. Leroux, D. Guyomard, and Y. Piffard, *Solid State Ionics* **80,** 299 (1995).
15. E. Zhecheva and R. Stoyanova, *Solid State Ionics* **66,** 143 (1993).
16. T. Ohzuku, A. Ueda, M. Nagayama, Y. Iwakoshi, and H. Komori, *Electrochim. Acta* **38,** 1159 (1993).
17. J. Gummow and M. M. Thackeray, *J. Electrochem. Soc.* **140,** 3365 (1993).
18. G. L. Che, B. B. Lakshmi, E. R. Fisher, and C. R. Martin, *Nature* **393,** 683 (1998).
19. F. Schlottif, M. Textor, U. Gerrgi, and F. Roewer, *J. Mater. Sci. Lett.* **18,** 599 (1999).
20. U. Gösele, A. P. Li, K. Nielsch, F. Muller, W. Erfurth, and R. B. Wehrspohn. Extended Abstract 158, 196th ECS Meeting, Toronto, Canada, 2000.
21. C. J. Brinker and G. W. Scherer, Sol–gel Science. Academic Press, New York, 1990.
22. L. L. Hench and J. K. West, *Chem. Rev.* **90,** 33 (1990).
23. M. A. Aegerter, R. C. Mehrota, I. Oehme, R. Reisfeld, S. Sakka, O. Wolfbers, and C. K. Jorgensen, "Optical and Electronic Phenomena in Sol–Gel Glasses and Modern Applications," Structure and Banding, Vol. 85. Springer-Verlag; Berlin, 1996.
24. B. B. Lakshmi, C. J. Patrissi, and C. R. Martin, *Chem.Mater.* **9,** 2544 (1997).
25. T. E. Huber, M. Sadoqi, J. A. Lubin, S. Manalis, and C. B. Prater, *Science* **263,** 800 (1994).
26. Y. Peng, H. L. Zhang, S. L. Pan, and H. L. Li, *J. Appl. Phys.* **87,** 7405 (2000).
27. S. L. Pan, H. L. Zhang, Y. Peng, Z. Wang, and H. L. Li, *Chem. J. Chin. Univ.* **20,** 1622 (1999).
28. C. Deimas and I. Saadoune, *Solid State Ionics* **53-56,** 370 (1992).
29. A. Ueda and T. Ohzuku, *Solid State Ionics* **141,** 2010 (1994).
30. T. Ohzuku, A. Ueda, M. Nagayama, Y. lwaoshi, and H. Komory, *Electrochim. Acta* **38,** 1159 (1993).
31. R. Stoyanova, E. Zhecheva, and L. Zarkova, *Solid State Ionics* **73,** 233 (1994).
32. L. A. Montoro, M. Abbate, and J. M. Rosolen, *J. Electrochem. Soc.* **147,** 1651 (2000).
33. Z. Y. Tan, "Photoelectron Energy Spectroscopy Analysis," Chap. 3. Dalian University of Technology Publishing Company, 1991.